DRAFT
Expected performance of type-Bp SAS in bKAGRA

December 27, 2016

Yoshinori Fujii

Table of Contents

1 Expected performance of type-Bp SAS in bKAGRA

As described in the previous section, the suspension system for the PR mirrors are upgraded toward bKAGRA from that was used in the iKAGRA period. This new system is called type-Bp SAS, and three of them are to be installed at the site. This chapter describes the type-Bp SAS system, its controllability, and the expected performance.

1.1 Overview

The mechanical overview of the type-Bpp SAS and the type-Bp SAS are shown in figure 1.1. The type-Bp SAS has two GAS filters to reduce coupling level from vertical to longitudinal vibration at higher frequency than 10 Hz. One recoil mass is also added at BF level with some sensor and actuator units called BF-LVDTs. It is suspended from beneath of the SF. This BF recoil mass (BR) system is aimed at damping main pendulum resonant modes by monitoring relative motion between the BF and the BR.

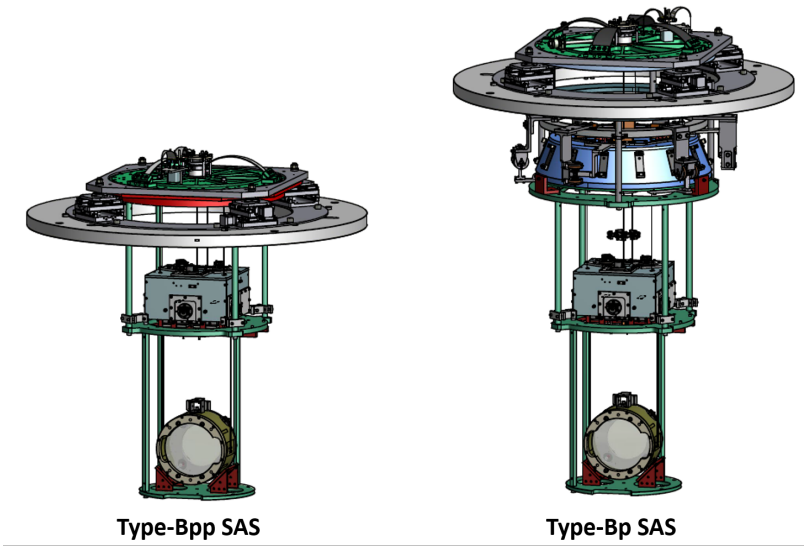

Figure 1.1: Mechanical overview of the type-Bpp SAS and the type-Bp SAS.

In addition, OSEM units are modified for risk reduction. For the IM-OSEM units, interval between LED and photo diode in IM-OSEMs are widened. While for the TM-OSEM units, the implemented sensors are removed from the type-Bp SAS and their long flags are replaced into shorter ones. Thence the type-Bp SAS has only optical length sensor and optical lever as the TM sensing system. Actuation system at TM level by TM-OSEMs remains.

This chapter focus on detailed mechanics of the type-Bp SAS and its active control system in each phase. Chapter 1.2 describes the detailed mechanical design of the type-Bp SAS. The newly added sensor and actuator units are explained in chapter 1.3. Chapter 1.4 presents the expected vibration isolation performance of the type-Bp SAS with active control system, and the control noise couping into the TM.

1.2 Mechanics

This section explains the mechanics of the suspension system and the related structures. Most of the environment is same as that of the type-Bpp SAS. Thence, this section especially focuses on the newly modified points. The suspension system is inside the vacuum chamber, and is surrounded by the extended security frame. The base of the suspension system is located on the inner frame inside the vacuum chamber. The inner frame stands on the ground.

1.2.1 Suspension system overview

The detailed type-Bp suspension system is shown in figure 1.2. The suspension system of the payload is same as that of type-Bpp SAS. The payload includes the test mass (TM), the recoil mass (RM), the intermediate mass (IM), and the intermediate recoil mass (IR). The BF and the payload are suspended from above system by single wire. The BF recoil mass (BR) is suspended from base of the standard GAS filter(SF) by three maraging rods. The suspension wire connecting the components above the IM are made of maraging steel. In the type-Bp SAS, the SF is supported by the traverser which conducts initial position alignment. the traverser stands on the top surface of the inner frame.

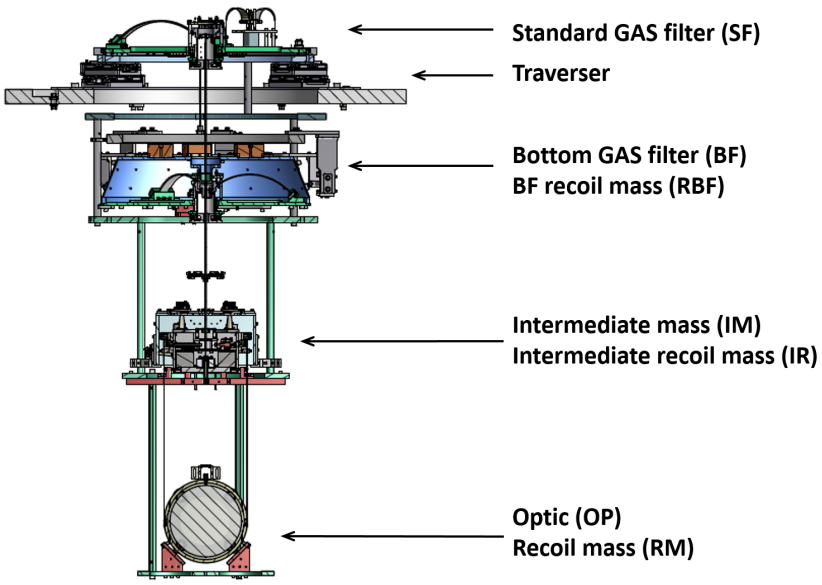

Figure 1.2: Ovweview of the type-Bp SAS.

1.2.2 Security frame

1.3 Sensors and actuators

The newly added sensors and actuators are explained in this section.

1.3.1 BF-LVDT

1.3.2 Wide cavity OSEM

1.3.3 Optical length sensor

1.4 Expected performance

The simulated performance of the newly designed type-Bp SAS is described in this section. This section includes the expected frequency responses of the suspension system, and its vibration isolation performances when the active controls are implemented. The modeled high noise seismic vibration at CLIO site is assumed in this simulation. According to the measured seismic vibration at KAGRA site, it seems to have shallow peak at around 2 Hz, while the vibration at the CLIO site does not have the structure. However, there is still no statistical measurement of the seismic vibration at KAGRA site and also the peak does not contribute a lot for current designing active control system. Thence the model obtained from measurement of CLIO site is used in this simulation, instead of the vibration of KAGRA site. In addition, optimally suspended system is also assumed. There is no horizontal discrepancy between the suspension point and the center of mass for each suspended mass.

The active control system is constructed so that the controls meets the requirements explained in chapter **??**, by considering the expected transfer functions of the suspension system described in chapter 1.4.1. The designed servo filters and the expected vibration isolation performances for the each control phase are described in chapter 1.4.2 to 1.4.4.

In following figures, the variable names of L, T, V, R, P, Y are used for expressing the DoFs of the vibration in this section. They are the first letter of the direction of the vibration (longitudinal, transversal, vertical, roll, pitch, yaw). The following two letters describes the name of the rigid bodies in the suspension system.

1.4.1 Suspension mechanical response

The mechanical responses of the type-Bp SAS is explained in this section explains. Figure 1.3 to figure 1.7 show the expected diagonal transfer functions from the implemented actuators to the sensors. According to the previous investigation, explained in chapter **??** and [], these predicted transfer functions are expected to fit well with the measurement below around 30 Hz for the measurements with OSEMs, and below around 5 Hz for the measurements with LVDTs. Except for the points, measurements are expected to follow these predicted transfer functions in this section.

The transfer functions in this section are fed back to the servo filter designs. The resonant frequencies of the type-Bp SAS are summarized in table 1.1, and their eigenmode shapes are shown in appendix A.

Diagonal transfer functions

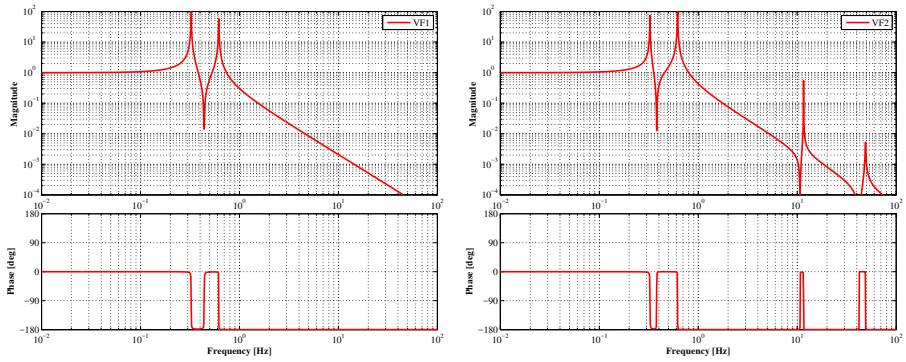

Figure 1.3: Diagonal transfer function measured by GAS-LVDTs.

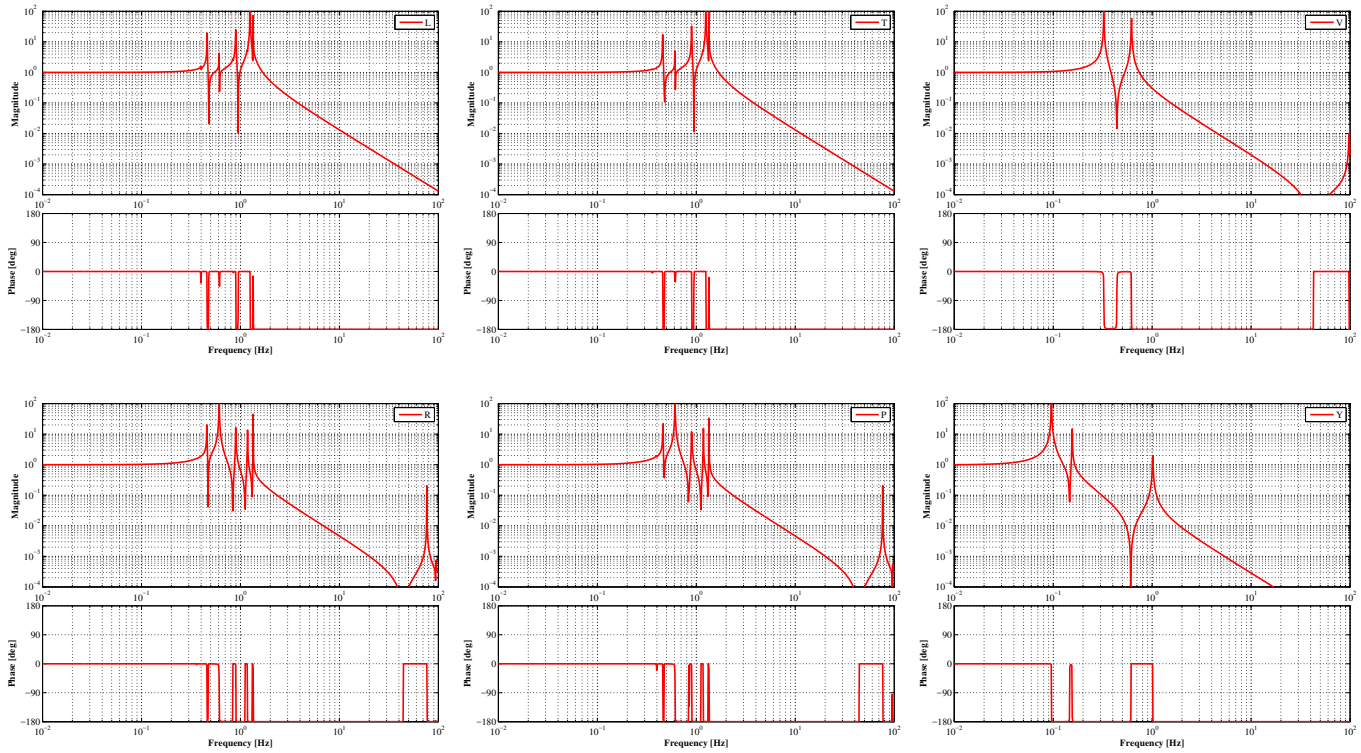

Figure 1.4: Diagonal transfer functions measured by BF-LVDTs

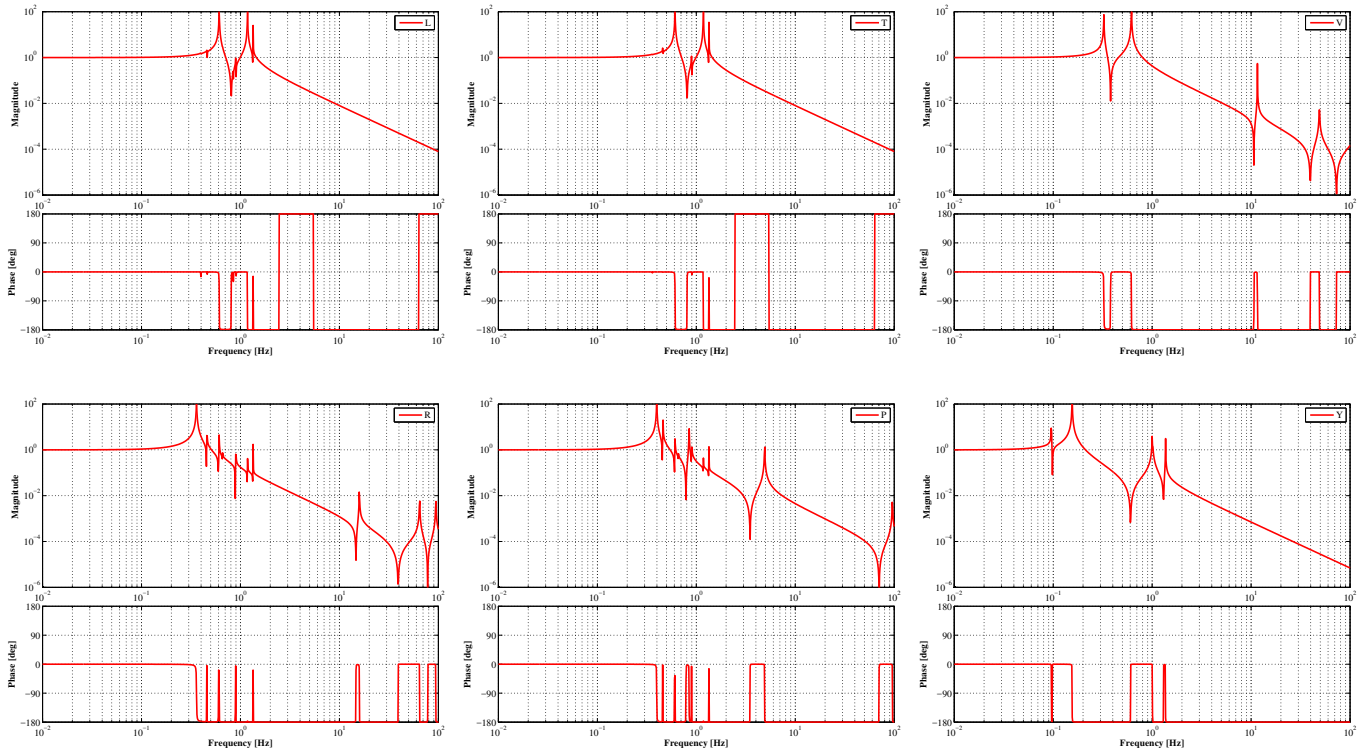

Figure 1.5: Diagonal transfer functions measured by IM-OSEMs

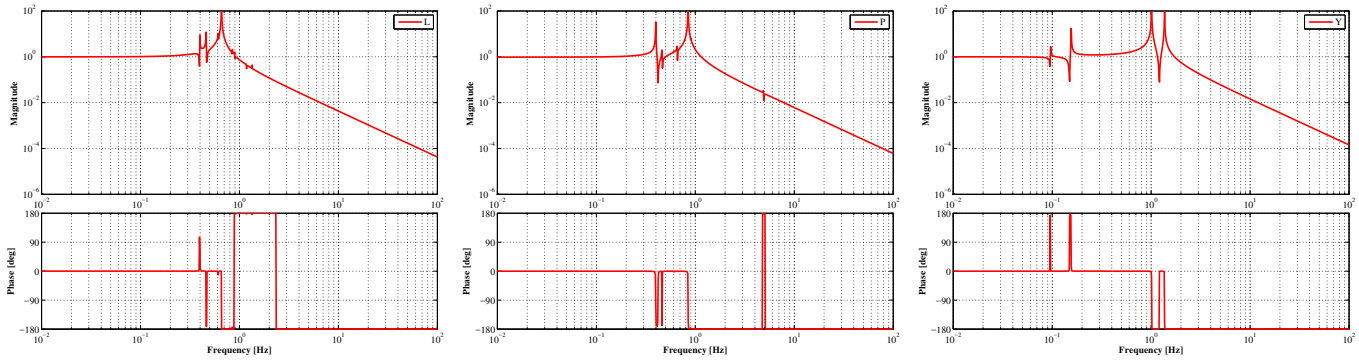

Figure 1.6: Diagonal transfer functions from oplevs to TM-OSEMs.

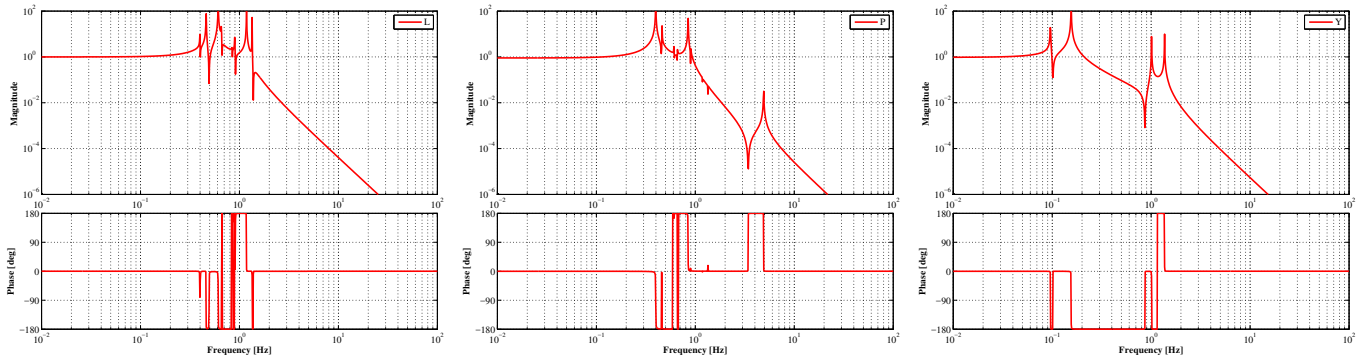

Figure 1.7: Diagonal transfer functions from oplevs to IM-OSEMs.

Eigenmodes from 3D rigid body model

#Mode No.	Frequwncy [Hz]	Mode shape	Note
#1	0.1	YBF, YIR, YRM, YTM	wire torsion
#2	0.161	YIM, YRM, YTM	wire torsion
#3	0.325	VBF, VIR, VIM, VRM, VTM	GAS filter
#4	0.376	RIM, RRM, RTM	IM roll
#5	0.414	PIM, PRM, PTM	IM pitch
#6	0.459	-RIM, TRM, -RRM, TTM, -RTM	main pendulum
#7	0.463	PIM, PRM, PTM	main pendulum
#8	0.612	RBF, TIR, RIR	BF roll
#9	0.613	-PBF, LIR, PIR, PTM	BF pitch
#10	0.618	VBF, VIR, -VIM, -VRM, -VTM	GAS filter
#11	0.659	-PIM, -LRM, -PRM, LTM, -PTM	TM-RM pendulum
#12	0.659	-RIM, TRM, -RRM, -TTM, -RTM	TM-RM pendulum
#13	0.849	PTM	TM pitch
#14	0.9	TBF, -RBF, -RRM, TIM, -TRM, -TTM	main pendulum
#15	0.901	-PBF, -PIR, PIM, PRM, -PTM	main pendulum
#16	1.011	YIM, -YRM, YTM	TM yaw
#17	1.017	YIR	IR yaw
#18	1.022	YBR	BR yaw
#19	1.186	RBF, -TIR, RIR, TIM	main pendulum
#20	1.186	PBF, LIR, PIR, -LIM	main pendulum
#21	1.261	LBR	BR pendulum
#22	1.261	TBR	BR pendulum
#23	1.351	-RBF, TIR, -RIR, TIM	IM pendulum
#24	1.352	PBF, LIR, PIR, LIM	IM pendulum
#25	1.369	YIM, -YTM	TM yaw
#26	4.906	-PIM, PRM	RM pitch
#27	11.611	-VIM, -VRM, VTM	TM vertical
#28	15.924	RTM	TM roll
#29	48.97	-YIM, YRM	VRM
#30	64.629	-RIM, RRM	RIM
#31	78.843	PBR	BR pitch
#32	78.843	RBR	BR roll
#33	97.094	RIR	IR roll
#34	98.66	PIR	IR pitch
#35	100.617	VBR	BR vertical
#36	126.38	VIR	IR vertical

Table 1.1: Simulated eigenmode list of Type-B SASp for bKAGRA

1.4.2 Controls in the calm-down phase

This section describes the active damping servos in the calm-down phase. The designing filters, its damping performances, and the sensor noise coupling to the interferometer signals are included. The servo filters are designed from the transfer functions from the implemented actuators and the sensors which are shown above.

Servo filter design

The schematic control diagram in the calm-down phase is shown in figure 1.8. The damping controls are set at the BF and IM levels by using the BF-LVDT units, and IM-OSEM units. Resonances of the vertical GAS filter vibration are damped by the GAS-LVDT and coil-magnet actuator unit, which is implemented into the SF. DC servos are also included in the GAS filter control loops to suppress the thermal drift of the GAS filters. At the TM level, damping loops by the optical lever and optical length sensor are implemented to suppress the relative motion between RM and TM, even though they have narrow linear range. This is because the sensors to measure the TM motion in the type-Bp SAS are only them.

In this section, the performance in 2 cases are investigated. First option is the case when the optical lever and the optical length sensor are available. The other option is the case if they are not available. Figure 1.9 to 1.11 show the Bode-plots of the designed servo filters in the calm-down phase. The displacement signals obtained by OSEM sensors and LVDTs are converted into the velocities with differentiation filters to get the viscous damping forces. Then, the converted signals are sent to the actuators with appropriate gains. The feedback filters have gains which is proportional to frequency f, around the mechanical resonant frequencies to be suppressed. The SF control gain has larger gain at the low frequencies to compensate the thermal drift of the GAS filters. The gains at high frequencies are cut off by low pass Butterworth filters with certain frequencies. In this calm-down phase, the cut-off frequencies are set at the lowest ones where all the mechanical resonances are suppressed within the requirement.

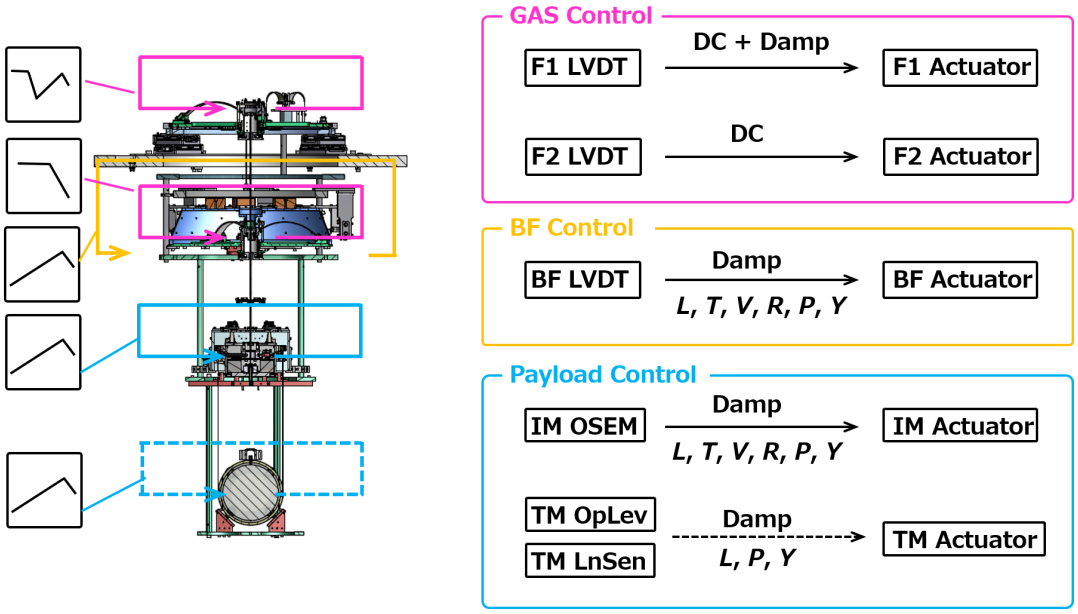

Figure 1.8: Control loops in the calm down phase.

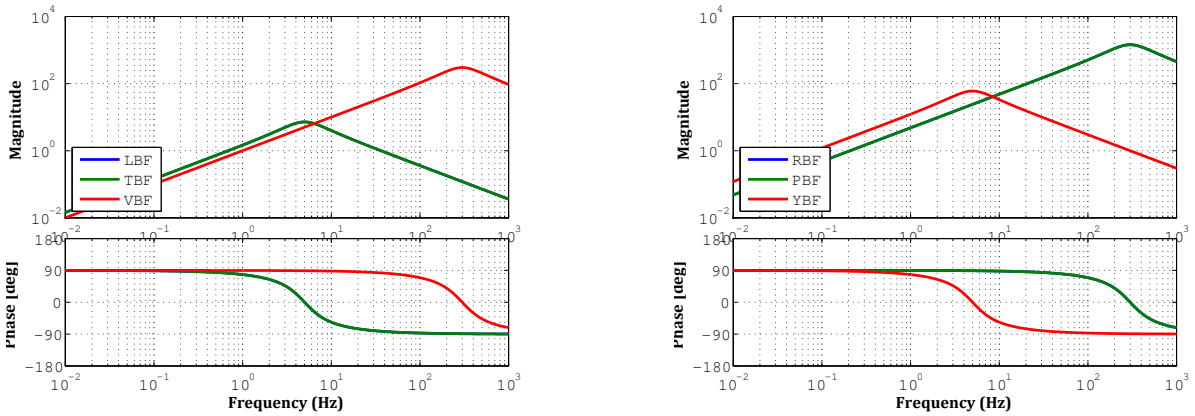

Figure 1.9: Servo filters for BF-level controls in the calm-down phase.

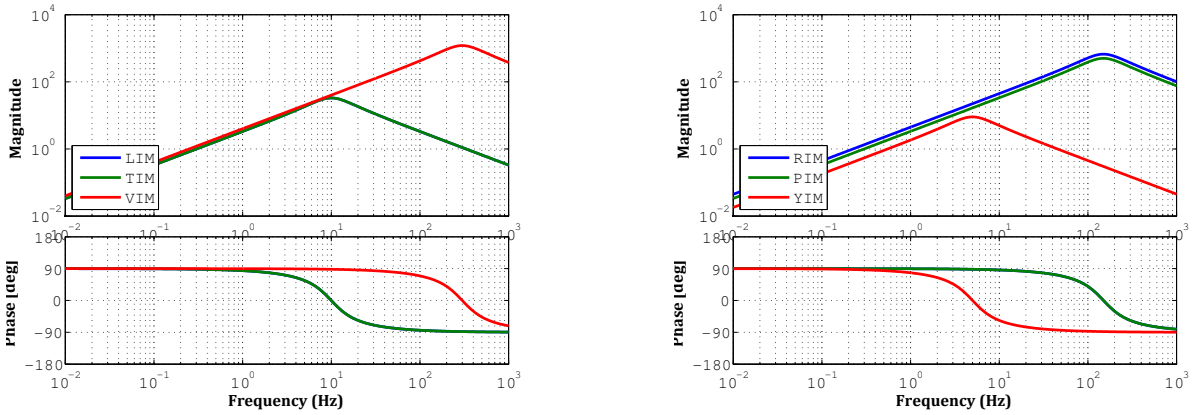

Figure 1.10: Servo filters for IM-level controls in the calm-down phase.

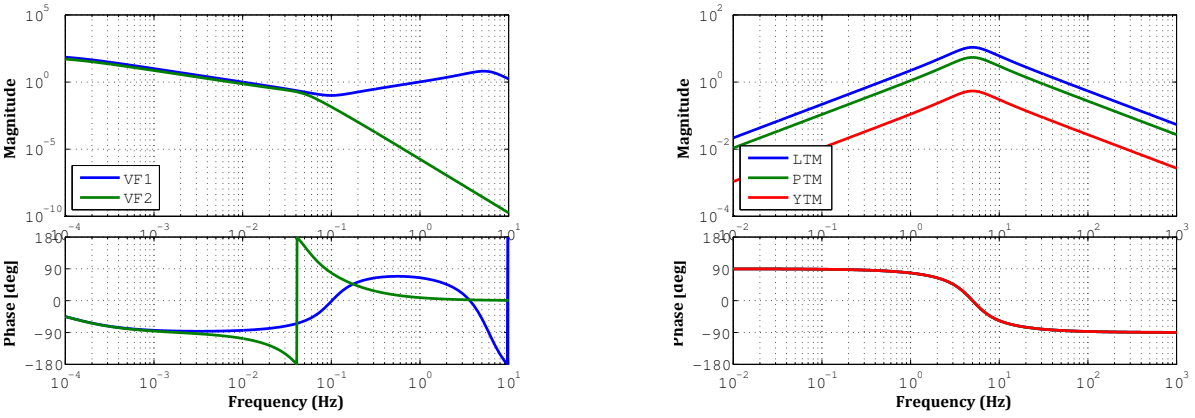

Figure 1.11: Servo filters for GAS controls ($Left$), for TM-level controls ($Right$) in the calm-down phase.

Expected damping performance

This section describes the performance of the damping control in terms of $1/e$ decay time of each mechanical resonance. $1/e$ decay time is a measure of the damping performance. The active control in this phase is required to damp the mechanical resonances with long decay time, especially at 0.1 Hz $\sim$ 1 Hz. The requirement for the decay time is to suppress the $1/e$ decay time to lower than 1 minute.

Figure 1.12 shows the expected $1/e$ decay time for each resonant frequency of the type-Bp SAS, with and without controls. The *Left* plot is the performance when the control loops with optical lever and optical length sensor at the TM level are opened, while the *Right* plot describes that when the control with these optical sensors are turned on. The former considers the optical sensors at the TM level are not available, while the latter supposes they are available. According to the plots in the former case, there are 3 resonant modes whose decay time exceed the requirement with active control, and according to the latter case, there is one such mode. Figure 1.13 shows those resonant mode shapes. All of these resonances are related with relative vibration between the TM and the RM in longitudinal, transversal and yaw DoFs, and thus to damp the resonances, sensing the TM motion is needed. If the optical sensors are available in the calm-down phase, the TM active control damps mode #11 and mode #16 (longitudinal and yaw DoF), which disturb the lock acquisition. On the other hand, the other mode #12 is not damped even if the TM controls are switched on, since there is no sensors and actuators for the TM motion in transversal DoF. However, the vibration which is related with the transversal DoF of the TM is not disturb the interferometer operation, unless its amplitude becomes larger than 1 mm. Thus there is no problem for this mode even if its decay time is larger than the requirement.

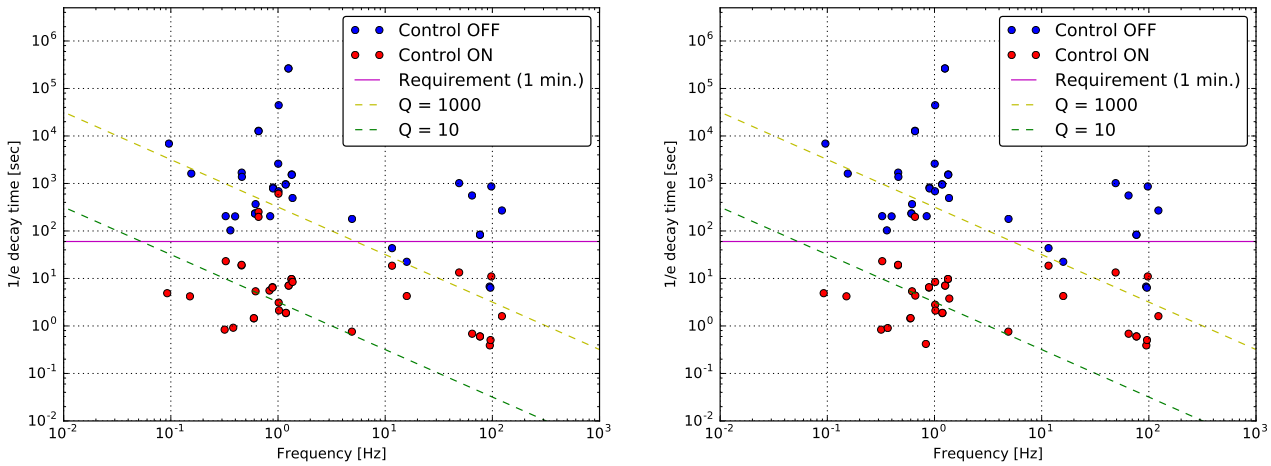

Figure 1.12: Expected $1/e$ decay time for each mechanical resonances in the type-Bp SAS with and without active control. *Left* shows the performance when the active control with optical sensors are not available, while *Right* describes that when the controls with the optical sensors are included.

In conclusion, if the optical sensors at TM level is available in the calm-down phase, the active controls damps all the mechanical resonances which disturb the interferometer operation, within 1 minute which is requirement for this controls. On the other hand, if the optical lever is not available in this phase, one has to wait 3 $\sim$ 10 minutes until the suspension system recovers its steady state.

Note that the angular fluctuation of the mirror is required to be suppressed lower than about 50 μrad to keep the optical lever within its linear regime. Such fluctuation can be excited by earthquakes and failure of lock acquisitions. Thence the details about the excited amplitude by external disturbances and frequency of such events is to be investigated.

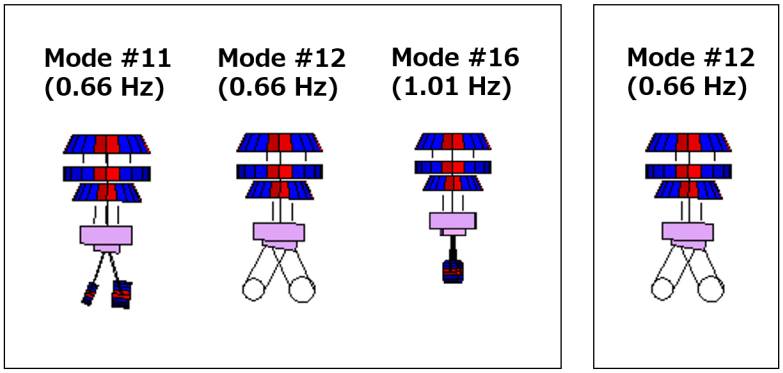

Figure 1.13: Mode shapes of the mechanical resonances whose $1/e$ decay time exceeds the requirement of 1 minute when the active control at TM level are not available (*Left*), while when the control with the optical sensors are working (*Right*). The $1/e$ decay time under this controls is expected around 200 sec for the mode #11, 250 sec for the mode #12, and 610 sec for the mode #16.

Sensor noise couplings in the calm-down phase

Figure 1.14 shows the expected noise couplings from each position sensor used in this control to longitudinal displacement of th TM. The considered noise sources are GAS-LVDTs, BF-LVDTs, and the optical sensors at TM level. In this simulation, it is assumed that there is no difference between the suspension position and the center of mass and thus no couplings from other DoF vibration due to mechanical asymmetry, as described above. The BF-LVDT, OSEM sensor, optical lever have 10^{-8} m$/\sqrt{\text{Hz}}$, 10^{-9} m$/\sqrt{\text{Hz}}$, and 10^{-7} rad$/\sqrt{\text{Hz}}$ for their noise level in the band of target gravitational waves, respectively. The displacement noise of the TM caused by the IM-OSEMs and optical sensors are much larger than the required level as shown in the plot. Thence the control with the OSEMs and the optical sensors should be excluded or modified in the observation phase. The control noise from BF-LVDT also violates the requirement at 11 Hz. Since the peak at 11 Hz is comes from a resonant vibration of the TM in vertical direction, the servos by BF-LVDTs and OSEMs are to be opened in vertical DoF, in the observation phase.

Table 1.2 shows the expected residual RMS values after the suspension system gets steady state. According to this table, all the simulated results meet the requirements for the calm down-phase controls. These predicted RMS values depend on mechanical Q factors of the resonant peaks, which have large uncertainty in this simulation. However, the actual mechanical Q factors of the KAGRA-SAS are either comparable with or lower than these predictions, comparing to the previous measurements. Thence the residual values of the actual suspension system is expected to be lower than the RMS. About yaw motion, this simulation does not include the prediction of its RMS, since predicting the precise yaw motion needs to consider asymmetry of the mechanical suspension system. There is also no detailed information about the asymmetry of the KAGRA-SAS. According to previous measurement which was done at TAMA site, where the magnitude of the seismic noise is much larger than that of the KAGRA site, its measured residual RMS of yaw motion was 40 μrad. Following these experiments, the amplitude of the residual yaw motion is expected to be lower than 40 μrad unless the suspension system has much asymmetries.

	displacement			velocity
Item	longitudinal [μm]	vertical [μm]	pitch [μrad]	longitudinal [μm/s]
Residual RMS	2.6	3.0	16.9	7.4

Table 1.2: Expected RMS values in the calm-down phase. The longitudinal, vertical, pitch displacement, and longitudinal velocity of the mirror are described in each column.

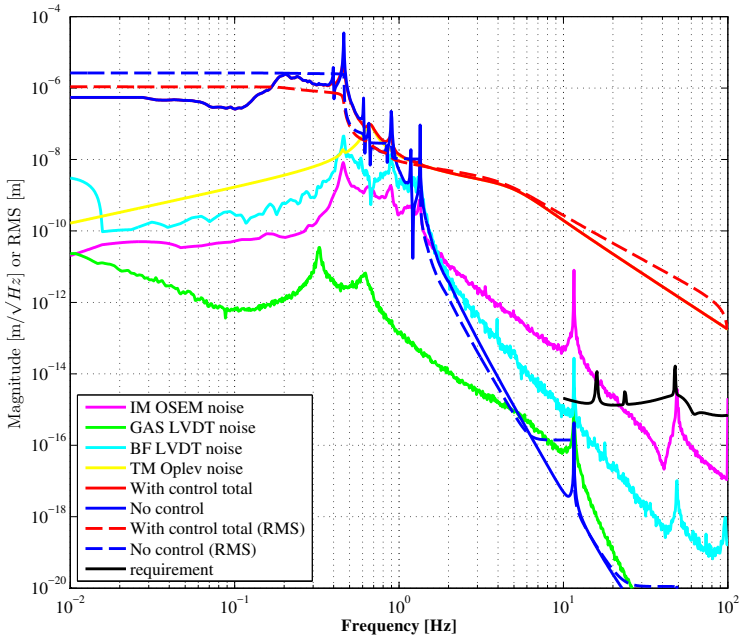

Figure 1.14: Expected sensor noise couplings to longitudinal displacement of the TM in the active controls in the calm-down phase. Tn the plot, optical sensors are included into the control. This plot includes the noise coupling from IM-OSEMs (magenta), from GAS-LVDTs at SF and BF (green), from BF-LVDTs (cyan), optical sensors at TM level (yellow). The total control noise (red), passive performance (blue) are also plotted. The dashed lines describe the RMS of total control noise and passive performance, down to 10^{-2} Hz.

1.4.3 Controls in the lock-acquisition phase

The aim of the control in the lock-acquisition phase is to suppress the RMS longitudinal velocity and RMS angular motion of the TM for the lock acquisition of the interferometer. Figure 1.15 shows the schematic diagram of this control phase. This active control is switched on, after the suspension system gets steady state.

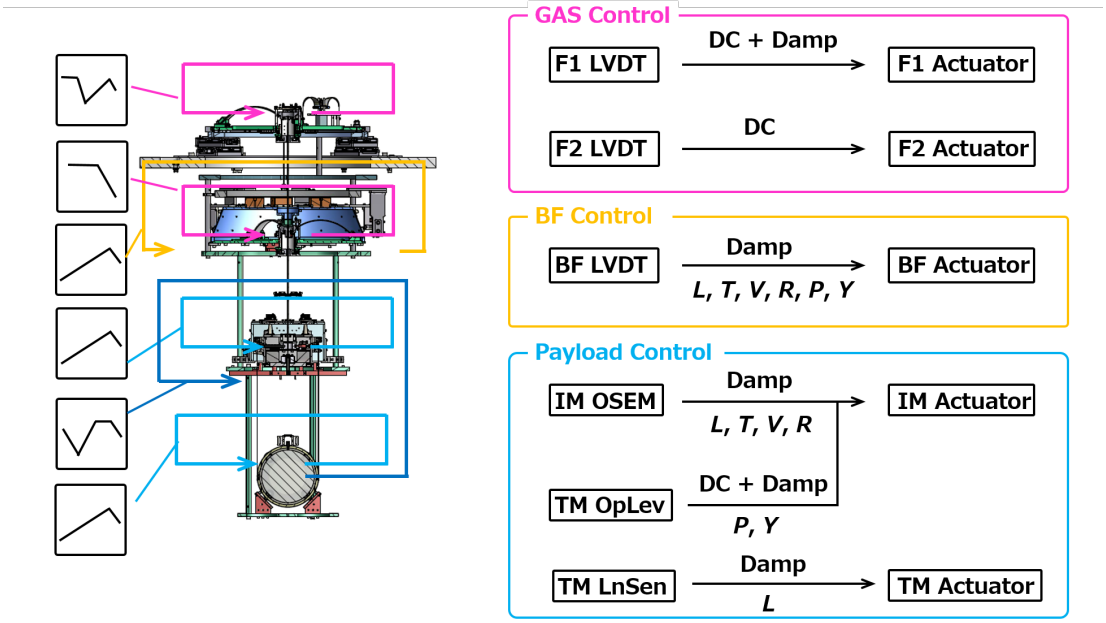

Figure 1.15: Control loops in the lock-acquisition phase.

In this phase, control loops for the payload are changed. Since important role of this phase is aligning the TM for the interferometer lock, both of DC and damping servos are implemented in the mirror pitch and yaw motion. In this alignment control for the mirror angular motion is achieved by the alignment controls with the optical lever. The signals of mirror pitch and yaw vibration are measured by the optical lever, and are fed back to the actuators implemented at IM level. The damping filters for pitch and yaw vibration by IM-OSEMs are turned off when the controls with optical lever are switched on. This is aiming at avoiding competition between the optical lever control and OSEM one.

Figure 1.16 to 1.18 show the Bode-plots of the designed servo filters in the lock-acquisition phase. The cut-off frequencies for the damping filters by BF-LVDTs and IM-OSEMs are set at ones where the resonances, which contribute to the RMS displacement of the mirror vibration, are efficiently damped. Figure 1.18 *Right* shows the servo filters for aligning the TM of suspended by the type-Bp SAS. The shapes of the servos are aimed at compensating the phase delay of the mechanical system. In these filters, DC servos are implemented at low frequencies for the mirror alignment. At the region between around 0.1 Hz to the unity gain frequencies ($\sim$ 2 Hz), the servo gains are raised by proportional to f^3 to compensate the phase delay due to the mechanical response. This is because the amplitude of the mechanical response gets smaller by proportional to f^{-4} and its phase delays 360 deg at high frequencies. The notch filter at 4.9 Hz in the pitch servo is included to avoid the instability of due to the mechanical response related with the pitch vibration of the recoil mass.

The expected RMS of longitudinal displacement, velocity and pitch angular displacement in this controls are described in table 1.3. It is confirmed that the active controls for this phase are met with the requirements. The RMS of TM yaw motion is not calculated, however, according to the previous measurement, it is expected to meet the requirement.

Servo filter design

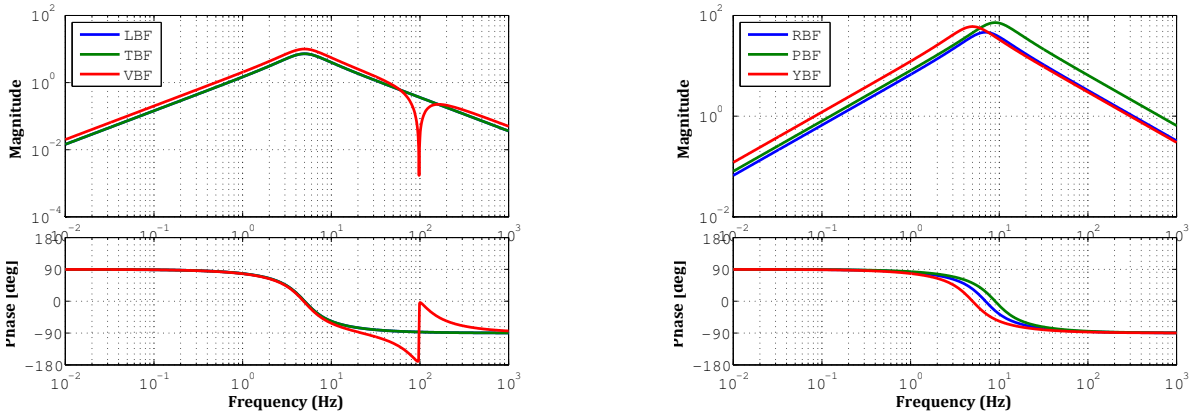

Figure 1.16: Servo filters for BF level controls in lock acquisition phase.

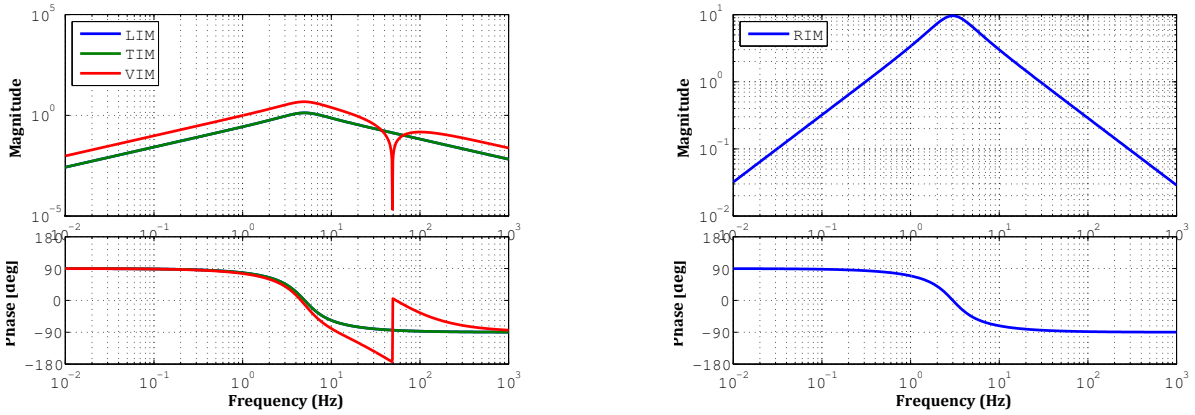

Figure 1.17: Servo filters IM level controls in lock acquisition phase.

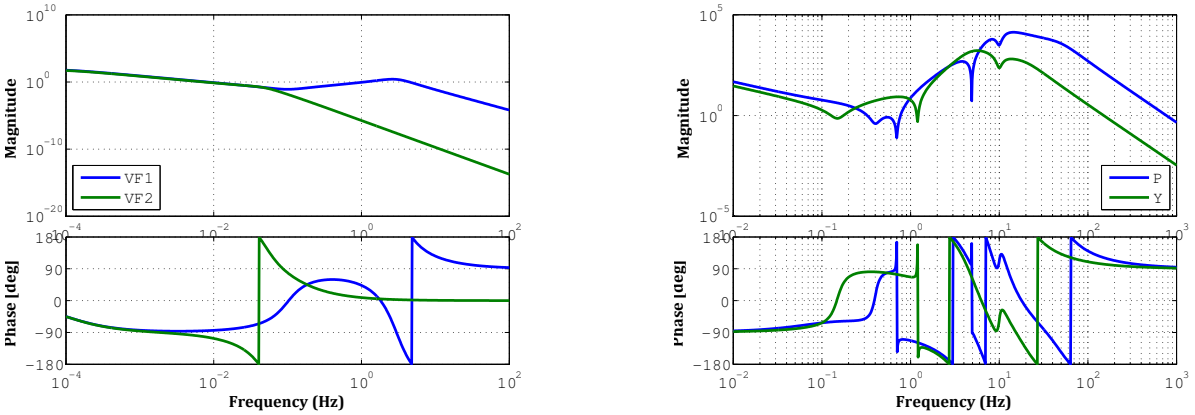

Figure 1.18: Servo filters for GAS controls ($Left$), for TM-level controls ($Right$) in lock acquisition phase.

Item	displacement [μm]	velocity [μm/s]	pitch [μrad]
Without controls	2.6	7.4	16.9
With controls	1.0	2.3	1.9

Table 1.3: Expected RMS of residual vibration in the calm down phase. The longitudinal displacement, longitudinal velocity, and pitch vibration of the mirror are described.

1.4.4 Controls in observation phase

The most important role of the control in the observation phase is to suppress the displacement noise lower than the requirement at 10 Hz, keeping the requirements on the RMS. The servo filters shown in this section are also used in the observation phase. After the lock-acquisition phase, only the optical lever is to be changed into the wave front sensor (WFS) to reduce the noise level at the target gravitational wave band.

Since the BF-LVDTs and IM-OSEMs have large sensor noises, the control by these sensors are wanted to opened in the observation phase if lower noise coupling at above 10 Hz is needed. However, the loops for horizontal and angular DoFs by BF-LVDTs are not possible to open them in the type-Bp SAS control system. This is because the resonant modes which have large contribution to the RMS are the main pendulum motion at 0.45 Hz, which are the mode #6, #7 shown in appendix A, and they are to be damped with the controls by using BF-LVDTs. In addition, the active controls for vertical DoF by BF-LVDTs and OSEMs induce the vertical resonance of the TM at 11 Hz, and this vibration causes the violation of the displacement requirement, as shown in figure 1.14. Thus the vertical controls by them are to be opened in this phase.

Consequently, the available sensors and DoFs are BF-LVDTs except for vertical DoF, and IM-OSEMs for longitudinal, transversal, roll DoFs. This section describes 2 options for the controls in the observation phase based on the issues.

Control without IM-OSEMs

In this controls, the loops by IM-OSEMs are opened to avoid inducing TM longitudinal vibration due to their sensor noise. In addition, the vertical control by BF-LVDT is also excluded not to excite the peak at 11 Hz by its sensor noise. Consequently, this control includes DC and damping servos by GAS-LVDTs, damping filters by BF-LVDTs except for the vertical DoF, and DC and damping filters by WFS. Figure 1.19 describes the control diagram of this controls.

The expected control noise coupling into the TM longitudinal direction in this control is shown in figure 1.20. The dominant coupling in $1 \sim 10$ Hz region comes from the BF-LVDT controls, and is close to the requirement at 10 Hz. However, it is unavoidable unless the BF-LVDTs are used. If the amplitudes of the servos by the BF-LVDTs, even though one can have larger margin at 10 Hz, the loops fail to suppress the RMS pitch motion lower than the requirement. Table 1.4 explains the active control performance in this phase. All the described parameters meet the requirements.

Item	RMS displacement	displacement at 10 Hz	RMS pitch
With controls	1.1 μm	5×10^{-16} m/$\sqrt{\text{Hz}}$	1.8 μrad

Table 1.4: Expected performance in the observation phase. The longitudinal displacement, longitudinal velocity, and pitch vibration of the mirror are described.

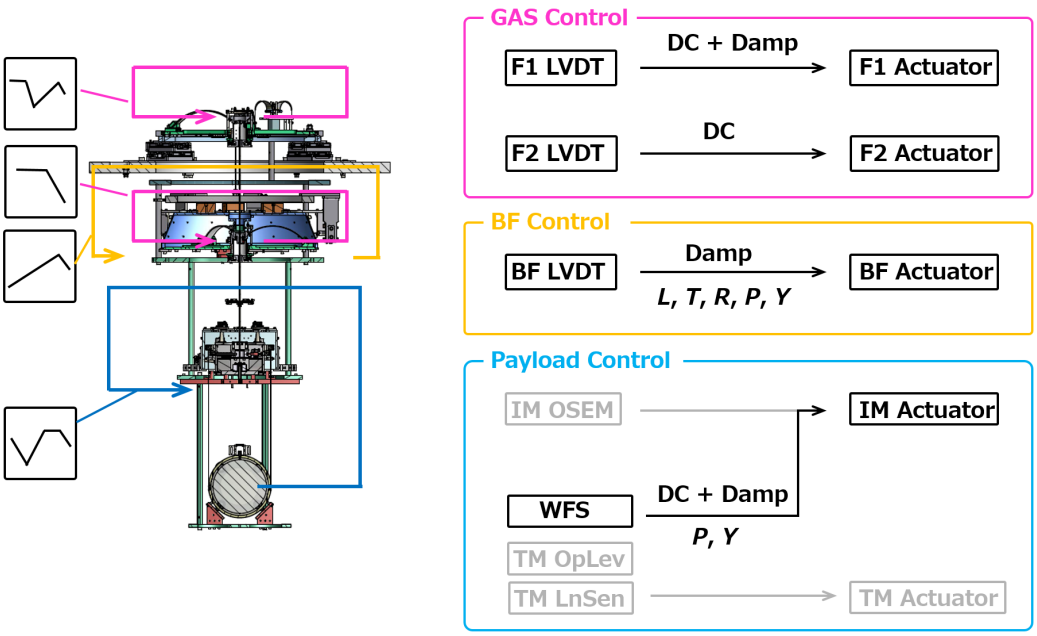

Figure 1.19: Control diagrams in observation phase without controls by IM-OSEMs.

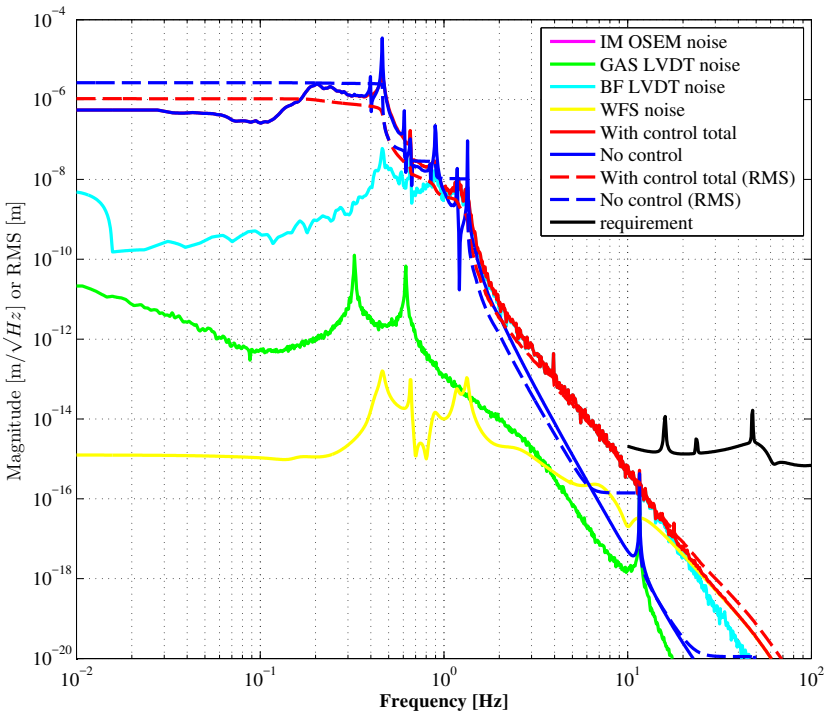

Figure 1.20: Control noise coupling to longitudinal displacement of the TM in the observation phase. This performance is obtained without IM-OSEM loops.

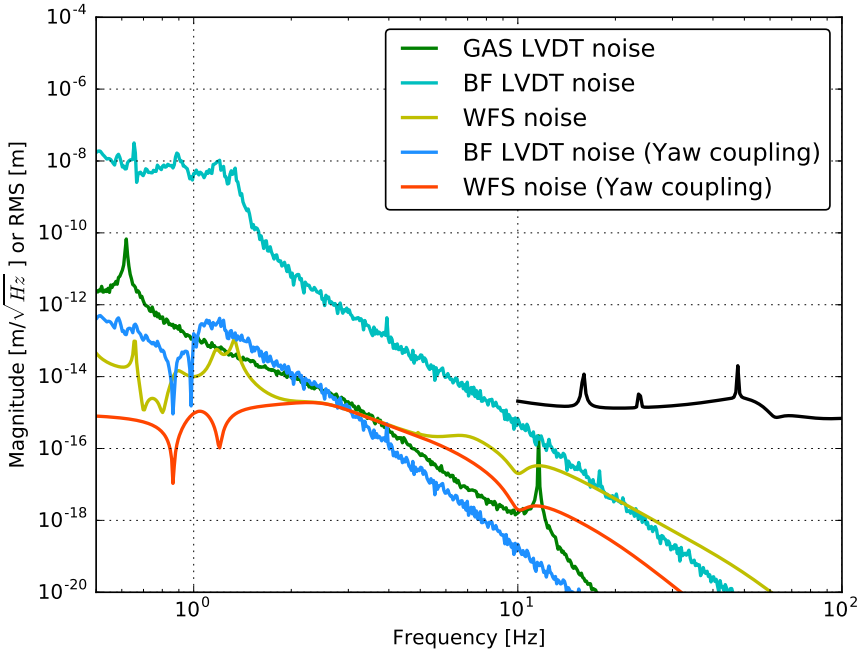

Figure 1.21: Control noise coupling due to 1 mm mis-centering of the beam spot. 2 curves (orange and blue) are added to the noise curves shown in figure 1.20. It assumes the system is optimally suspended, and also the beam spot at the mirror is shifted horizontally by 1 mm.

Figure 1.20 describes the performance when the interferometer beam is centered. However, the beam spot can be mis-centered in actual situation. If the beam is shifted horizontally, yaw DoF motion couples to longitudinal vibration. Figure 1.21 shows the the noise couplings from yaw motion of the mirror at around 10 Hz. It assumes that the interferometer beam is shifted by 1 mm from the center. According to the result, the yaw couplings due to the mis-centered of the beam by 1 mm is lower than the requirement and also the couplings from BF-LVDTs. Since its beam shift is aligned within 1 mm for the interferometer operation, the effect of yaw coupling due to mis-centering of the beam is not affect to the requirement.

Controls with IM-OSEMs

This section describes the controls including the IM-OSEM feed back loops for the observation phase. In above section, it is presented that the active controls without IM-OSEM controls meet the requirements. However, the actuation forces can excite resonance which disturbs the interferometer operation if there are couplings from other DoFs due to the imperfection of actuator diagonalization. If it happens, the vibration excited by the IM actuators can transmit to the TM directly. In this situation, including damping controls by IM-OSEMs would be useful to avoid exciting such resonances.

Figure 1.22 shows the diagram of this control. To avoid inducing the resonant peak at 11 Hz related with TM vertical vibration, the damping filters for vertical DoF at BF and IM are excluded. The loops for pitch and yaw DoF at IM are also opened to prevent from competition between the control by WFS and that by IM-OSEMs.

The expected noise coupling in this controls is shown in figure 1.23, and it includes the couplings from the TM yaw motion due to mis-centering of the interferometer beam by 1 mm. According to the simulation, the expected IM-OSEM control noise is lower than the requirement, even though it becomes dominant at above 10 Hz. The obtained RMS longitudinal displacement, RMS pitch vibration, and longitudinal displacement at 10 Hz are 1.0 μm, 1.8 μrad, and 8.5×10^{-16} m/$\sqrt{\text{Hz}}$, respectively. Since, the IM control cannot damp the main pendulum modes at 0.45 Hz, the RMS of them are not changed comparing to the other control system in the observation phase.

Consequently, it is possible for the type-Bp SAS to include the control loops by IM-OSEMs even in the observation phase. It is not needed to include the controls by the IM-OSEMs in the observation phase, however, it would be safer to use the IM-OSEM damping servos in this phase, from viewpoint of actual situation.

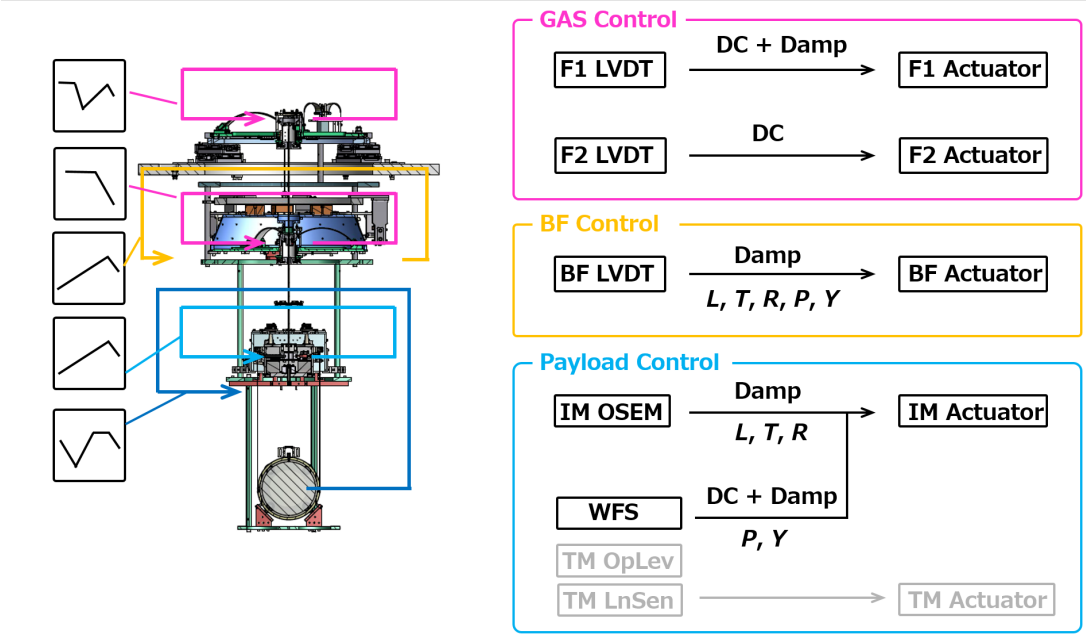

Figure 1.22: Control diagrams in observation phase with controls by IM-OSEMs.

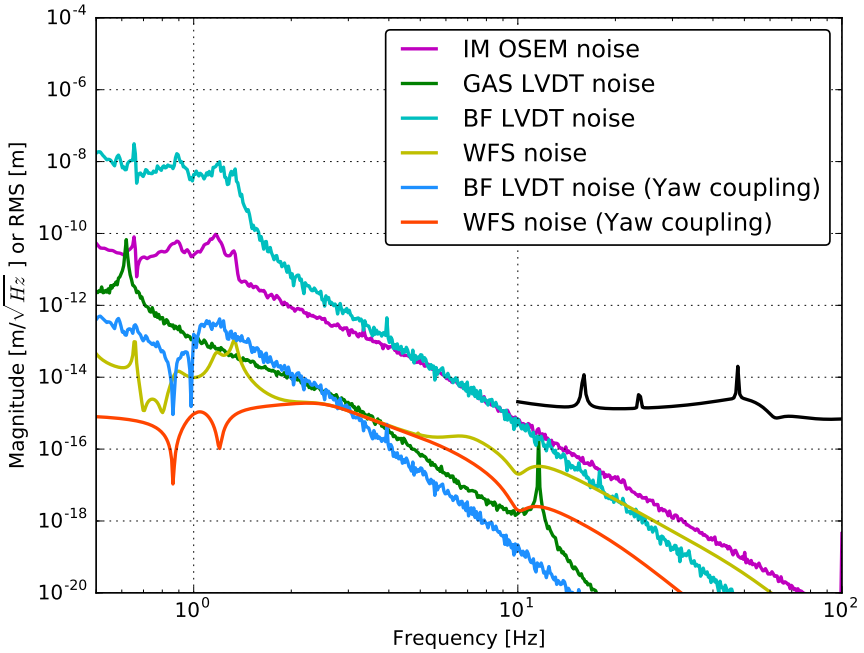

Figure 1.23: Control noise coupling to longitudinal displacement of the TM in the observation phase. This performance is obtained with IM-OSEM loops.

1.5 Conclusion

From the simulation in this chapter, it is confirmed that the designed active control system for the newly designed type-Bp SAS meets fundamental requirements which are set in chapter **??**. Table 1.5 summarizes the requirements which are set for the type-Bp SAS active control system and simulated performance. The prediction in yaw DoF is not included in this calculation, since there is no information about the mechanical asymmetry which the KAGRA-SAS typically have. However, it is expected that the active controls is able to clear the requirement for yaw motion, according to the previous experiments.

The problematic issue in the active control system for the type-Bp SAS is that it is required to use the optical sensors in the calm-down phase, which have narrow linear range. If the optical sensors are not available in the calm-down phase, one has to wait around 10 minutes, after failure of the lock acquisition of the interferometer or large earthquakes.

The calm-down phase			
Items	Requirements	Expected performance	ref.
$1/e$ decay time	< 1 min.	< 23 sec.	
(Residual) RMS displacement (longitudinal)	< 50 μm	7 μm	
(Residual) RMS displacement (vertical)	< 1 mm	3 μm	
(Residual) RMS angle (pitch)	< 50 μrad	17 μrad	
The lock acquisition phase			
RMS velocity (longitudinal)	< 5 μm/sec.	2.3 μm/sec	
RMS angle (pitch)	< 2 μrad	1.9 μm/sec	
The observation phase			
Control noise at 10 Hz (longitudinal)	$< 1 \times 10^{-15}$ m/$\sqrt{\text{Hz}}$	$5 \sim 8 \times 10^{-16}$ m/$\sqrt{\text{Hz}}$	
RMS displacement (longitudinal)	< 70 μm	1 μm	
RMS angle (pitch)	< 2 μrad	1.8 μrad	

Table 1.5: Fundamental requirements of the active controls for the type-Bp SAS and the expected performance.

A Eigenmodes of type-Bp SAS

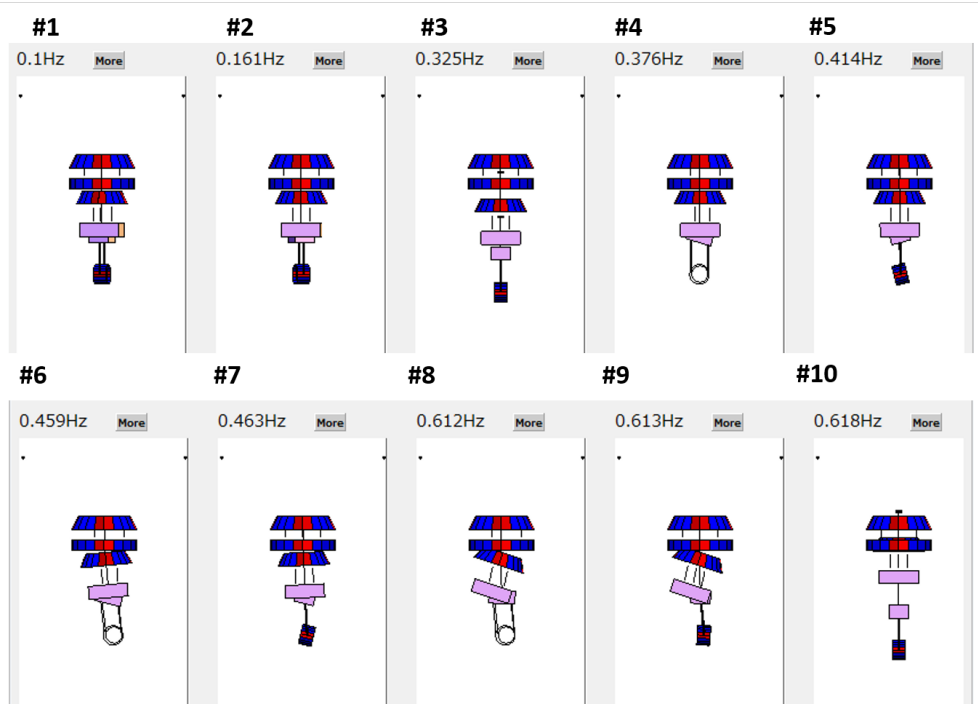

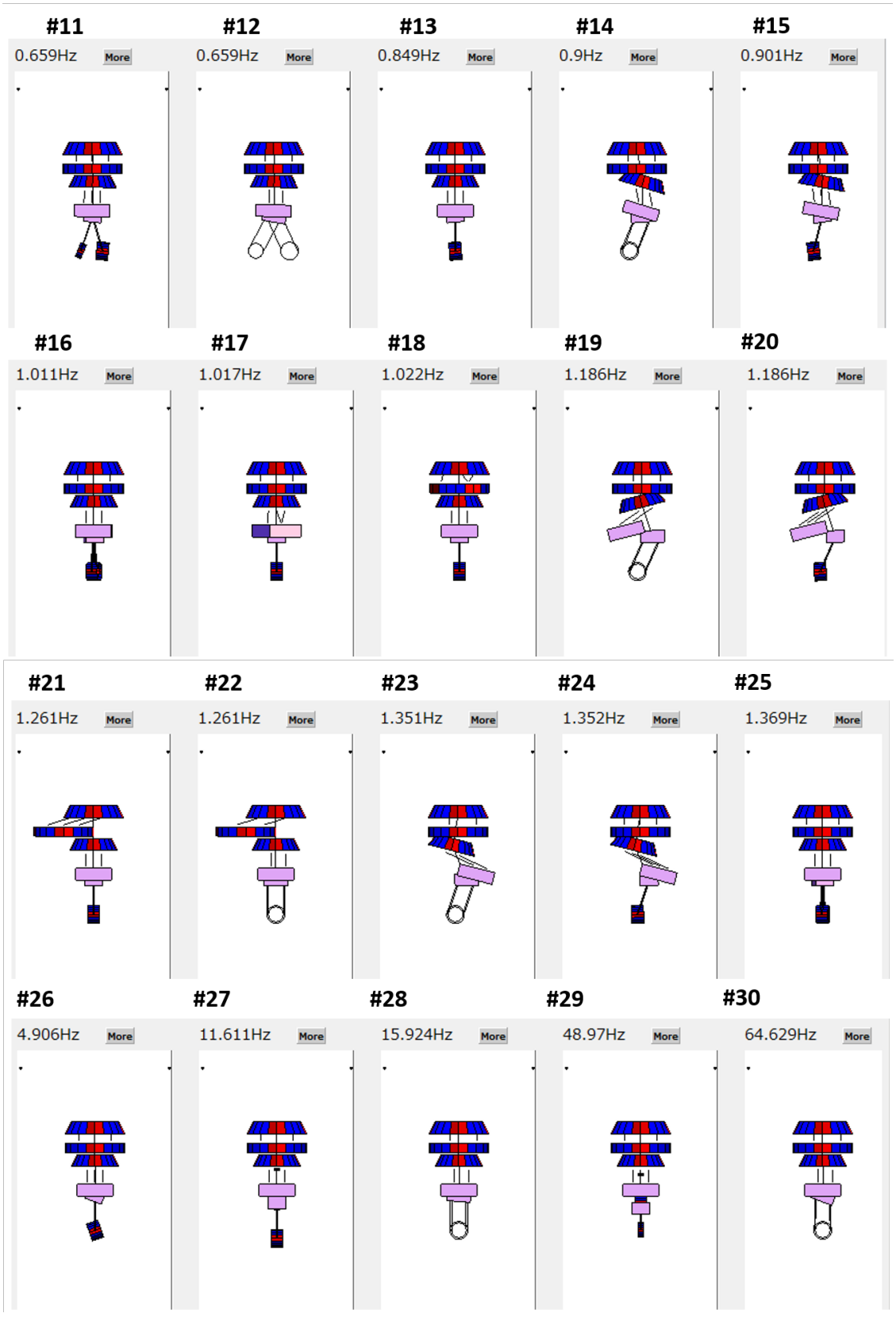
#11
0.659Hz
More
#12
0.659Hz
More
#13
0.849Hz
More
#14
0.9Hz
More
#15
0.901Hz
More
#16
1.011Hz
More
#17
1.017Hz
More
#18
1.022Hz
More
#19
1.186Hz
More
#20
1.186Hz
More
#21
1.261Hz
More
#22
1.261Hz
More
#23
1.351Hz
More
#24
1.352Hz
More
#25
1.369Hz
More
#26
4.906Hz
More
#27
11.611Hz
More
#28
15.924Hz
More
#29
48.97Hz
More
#30
64.629Hz
More

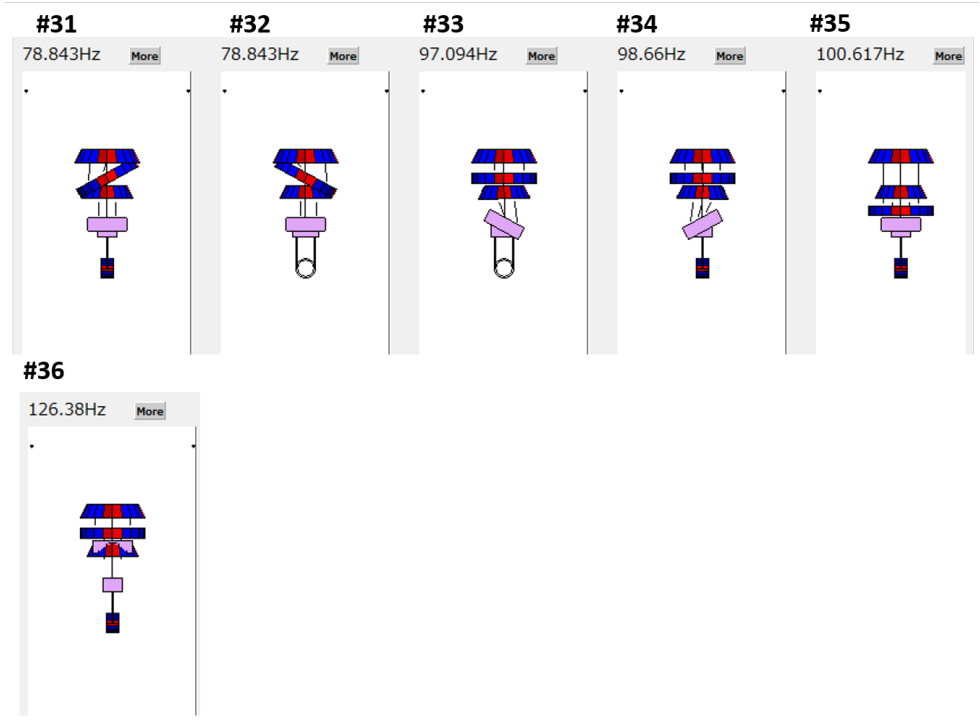
#31
78.843Hz
More
#32
78.843Hz
More
#33
97.094Hz
More
#34
98.66Hz
More
#35
100.617Hz
More
#36
126.38Hz
More

B Active control system for type-Bp SAS

B.1 Controls in calm-down phase

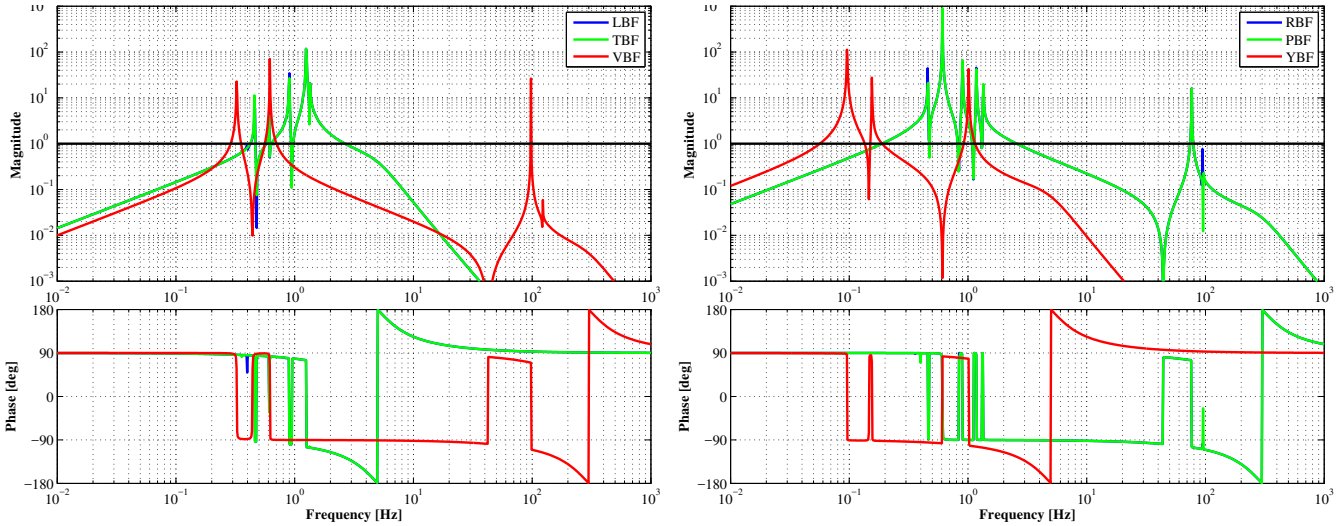

Figure B.1: Open loop transfer functions of active damping controls at BF level.

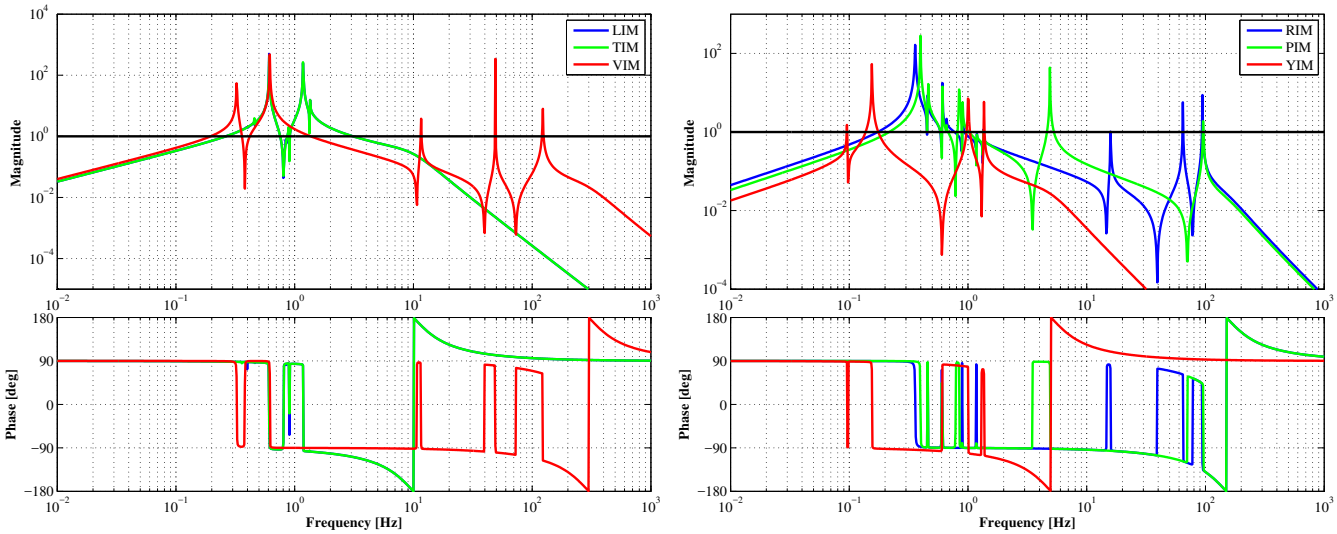

Figure B.2: Open loop transfer functions of active damping controls at IM level (*Right*).

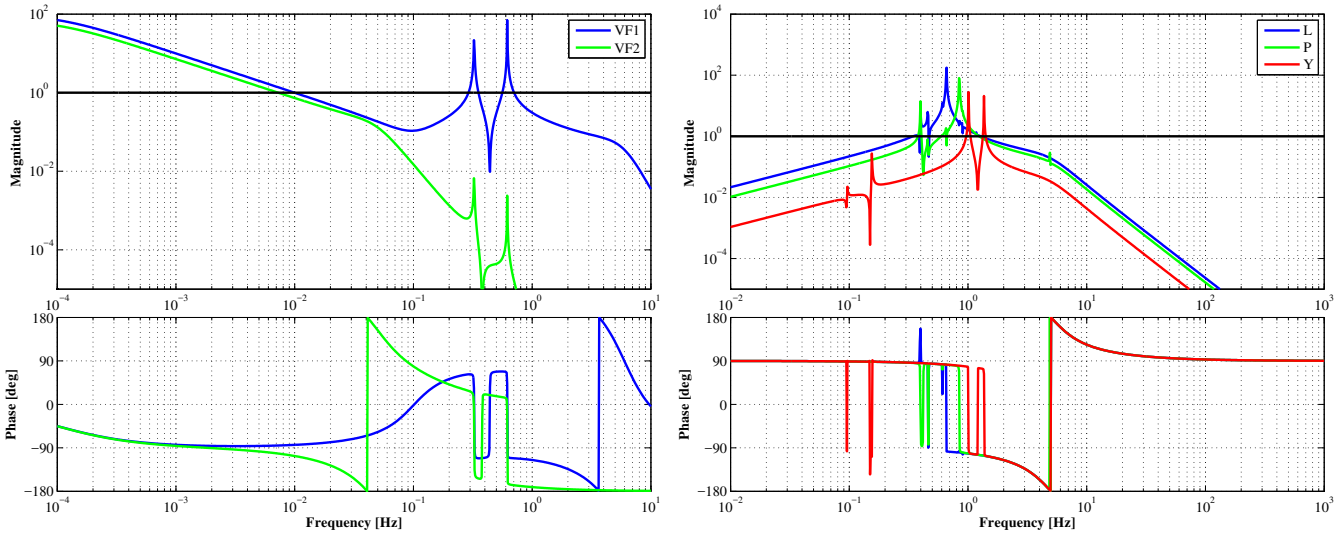

Figure B.3: Open loop transfer functions of active damping controls for GAS filters ($Left$) and at TM level.

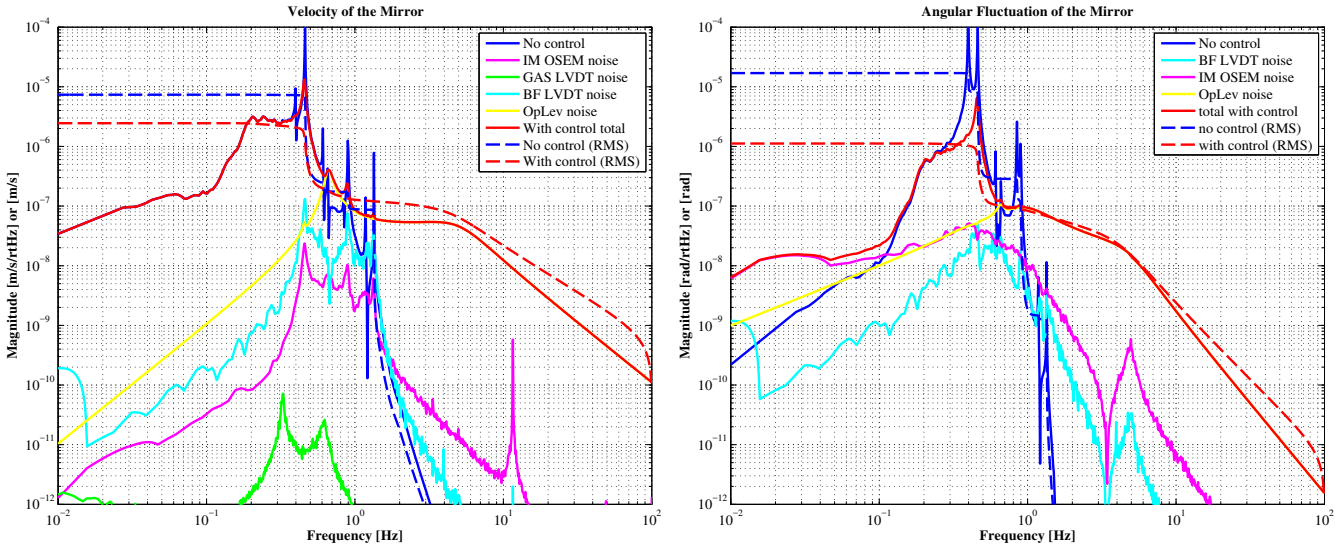

Figure B.4: Expected control noise coupling into longitudinal velocity fluctuation ($Left$) and into the pitch vibration ($Right$) of the mirror in the calm-down phase.

B.2 Controls in lock acquisition and observation phase

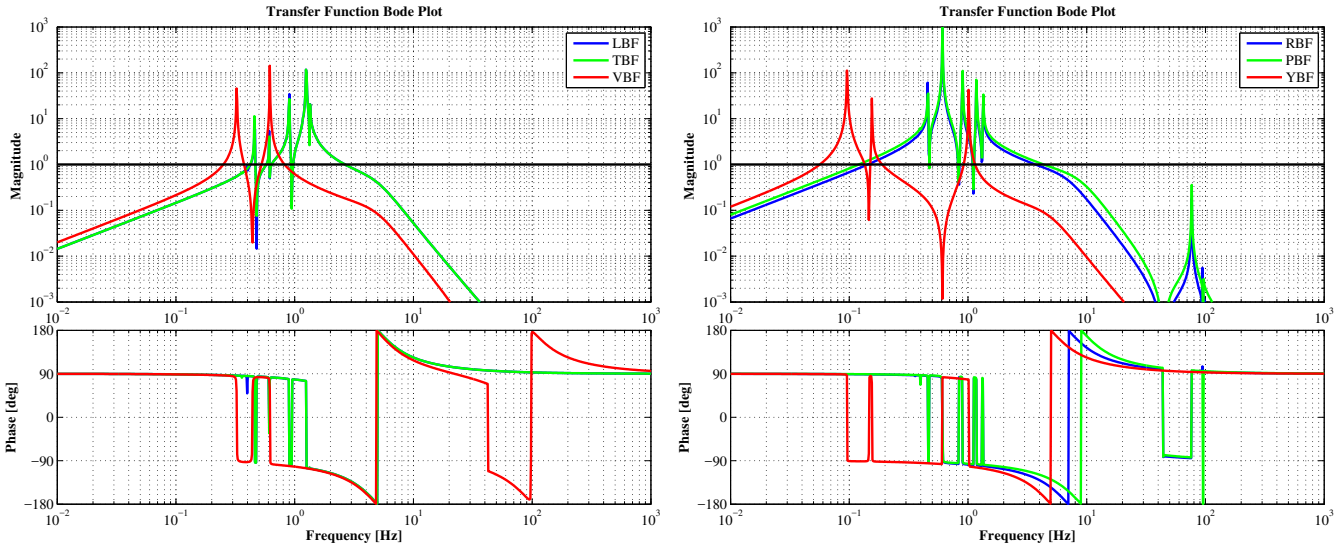

Figure B.5: Open loop transfer functions of active controls at BF level in the lock acquisition and the observation phase.

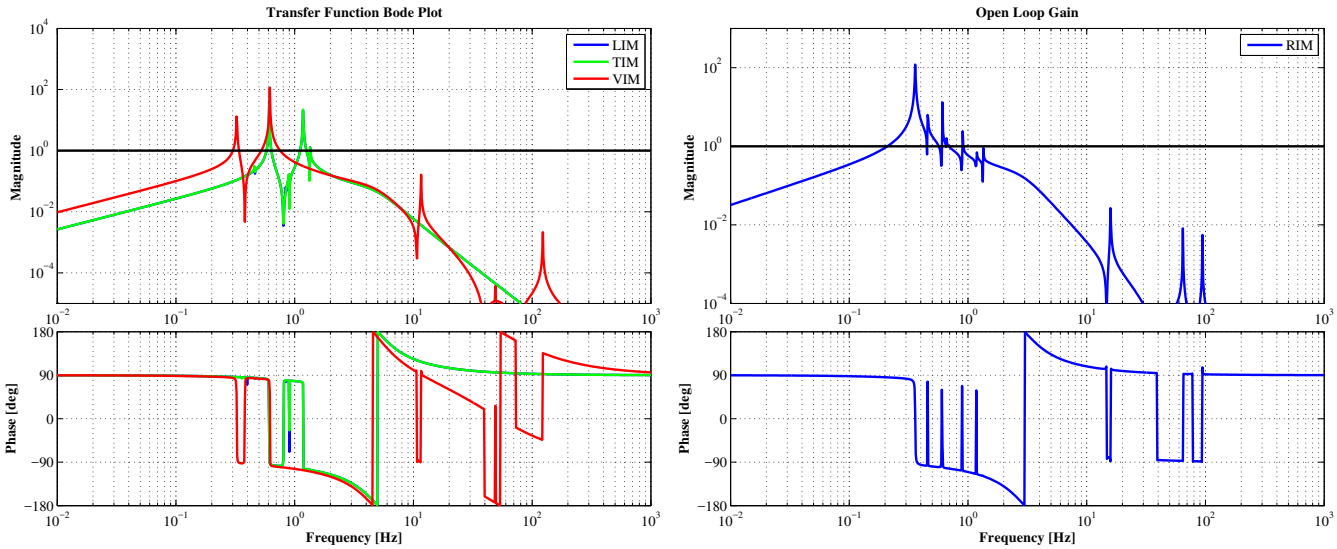

Figure B.6: Open loop transfer functions of active controls at IM level in the lock acquisition and the observation phase.

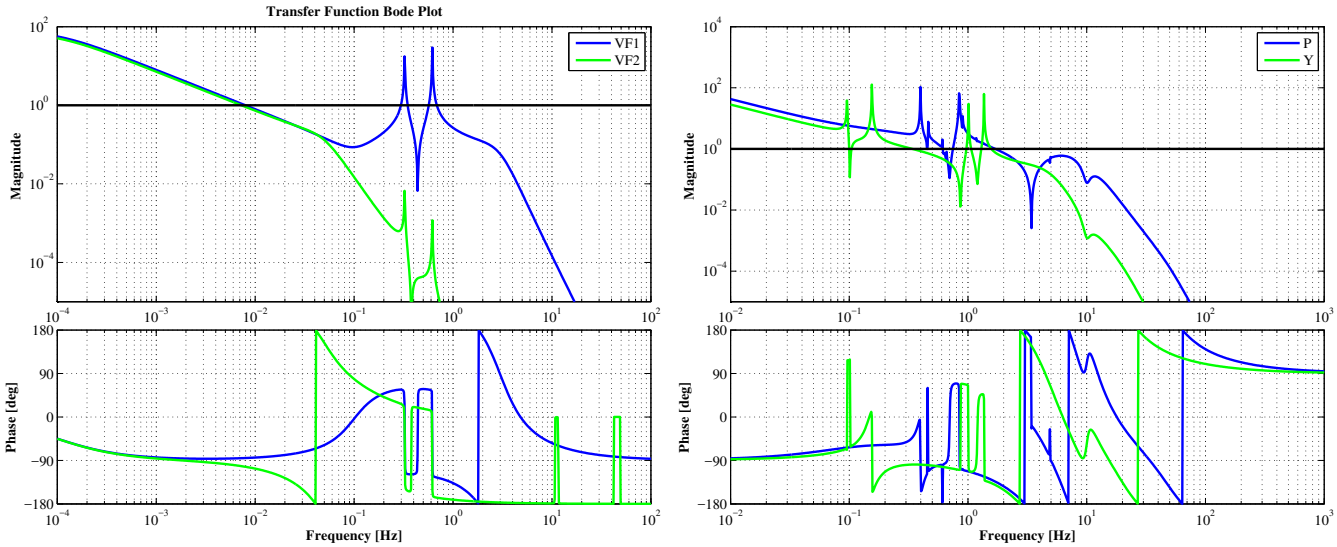

Figure B.7: Open loop transfer functions of active controls for GAS filters ($Left$) and at TM level in the lock acquisition and the observation phase.

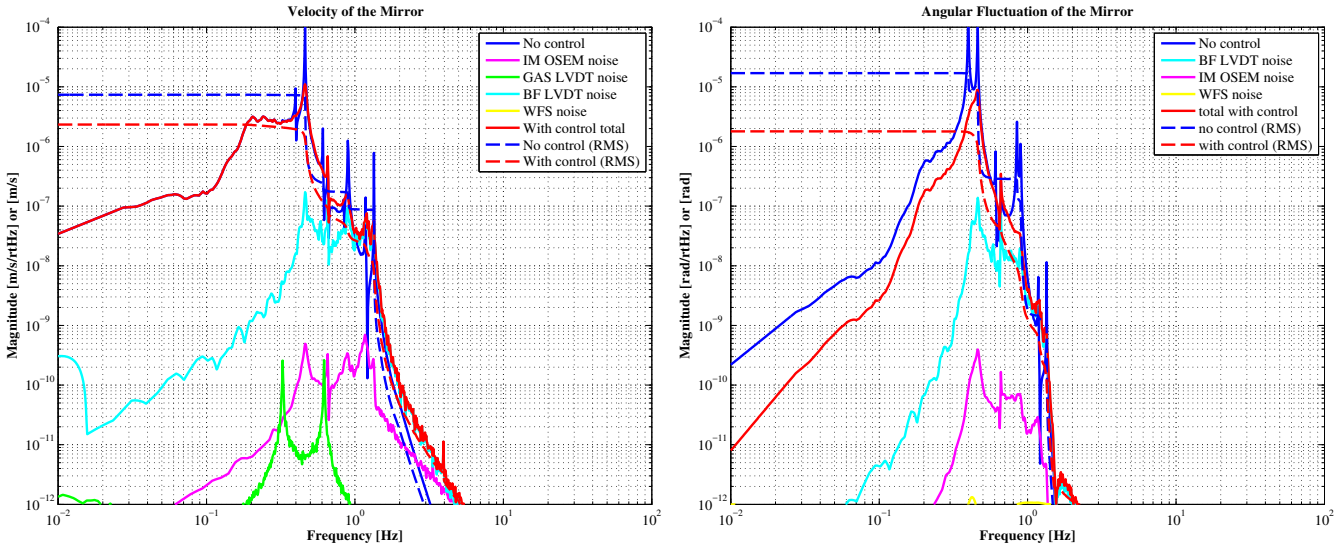

Figure B.8: Expected control noise coupling into longitudinal mirror vibration in velocity ($Left$) and into the pitch vibration ($Right$) of the mirror in observation phase.